THE JOURNAL OF PHYSICAL CHEMISTRY A
A JOURNAL OF THE AMERICAN CHEMICAL SOCIETY

pubs.acs.org/JPCA

Article

Benchmarking Charge-Transfer Excited States in TADF Emitters: ΔDFT Outperforms TD-DFT for Emission Energies

Published as part of The Journal of Physical Chemistry A virtual special issue "Gustavo Scuseria Festschrift".

Thomas Froitzheim,[‖] Lukas Kunze,[‖] Stefan Grimme, John M. Herbert, and Jan-Michael Mewes*

Cite This: *J. Phys. Chem. A* 2024, 128, 6324–6335

Read Online

ACCESS | Metrics & More | Article Recommendations | Supporting Information

ABSTRACT: Charge-transfer (CT) excited states are crucial to organic light-emitting diodes (OLEDs), particularly to those based on thermally activated delayed fluorescence (TADF). However, accurately modeling CT states remains challenging, even with modern implementations of (time-dependent) density functional theory [(TD-)DFT], especially in a dielectric environment. To identify shortcomings and improve the methodology, we previously established the STGABS27 benchmark set with highly accurate experimental references for the adiabatic energy gap between the lowest singlet and triplet excited states (ΔE_{ST}). Here, we diversify this set to the STGABS27-EMS benchmark by including experimental emission energies (E_{em}) and use this new set to (re)-evaluate various DFT-based approaches. Surprisingly, these tests demonstrate that a state-specific (un)restricted open-shell Kohn–Sham (U/ROKS) DFT coupled with a polarizable continuum model for perturbative state-specific nonequilibrium solvation (ptSS-PCM) provides exceptional accuracy for predicting E_{em} over a wide range of density functionals. In contrast, the main workhorse of the field, Tamm–Dancoff-approximated TD-DFT (TDA-DFT) paired with the same ptSS-PCM, is distinctly less accurate and strongly functional-dependent. More importantly, while TDA-DFT requires the choice of two very different density functionals for good performance on either ΔE_{ST} or E_{em}, the time-independent U/ROKS/PCM approaches deliver excellent accuracy for both quantities with a wide variety of functionals.

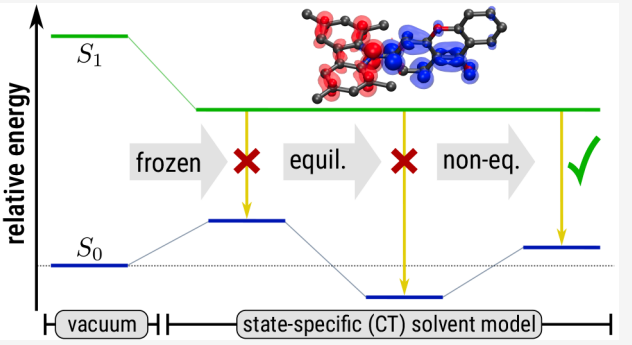

I. INTRODUCTION

The rise of computation-driven rational design in organic electronics and materials necessitates the robust and accurate prediction of optoelectronic properties.[2−8] Next-generation organic light-emitting diodes (OLEDs) based on thermally activated delayed fluorescence (TADF) are a prominent example. TADF emitters harvest both singlet and triplet excitons through the transfer of excitons via (reverse) intersystem crossing [(r)ISC]. Since the rate of population transfer depends exponentially on the adiabatic energy gap ΔE_{ST} between the lowest singlet (S_1) and triplet (T_1) excited states, it imposes a tight constraint on TADF emitter design. One way to achieve small singlet−triplet gaps on the order of the thermal energy ($k_BT \approx 0.025$ eV) is by spatially separating electron and hole in charge-transfer (CT) excited states. Accordingly, the computational study of CT states and the accurate prediction of their relative energies have attracted great interest.

To assess the accuracy of commonly applied methods for the CT state of TADF emitters, some of us previously introduced the STGABS27 benchmark set,[1] consisting of 27 emitters with highly accurate experimental ΔE_{ST} values obtained from temperature-dependent measurements of the TADF rate.[9] Our work demonstrated that state-specific restricted or unrestricted open-shell Kohn–Sham density functional theory (ROKS or UKS)[10−13] combined with a polarizable continuum solvation model (PCM)[14,15] yields ΔE_{ST} with a remarkably small error of ≈0.5 kcal/mol, which we attributed to the full inclusion of orbital relaxation and dielectric screening in the method. Note that by UKS, ROKS, and generally ΔDFT, we refer to SCF-based nonaufbau methods applied to open-shell singlet excited states and (as is more common) triplet states. In UKS for open-shell singlets, ground-state orbitals are manually repopulated to form a nonaufbau determinant, and converged using the maximum overlap method (MOM) to avoid variational collapse.[12] ROKS improves on UKS by correcting the spin-state of the open-shell singlet determinant through the introduction of a second (triplet) determinant in the same

Received: May 17, 2024
Revised: July 4, 2024
Accepted: July 5, 2024
Published: July 19, 2024

orbitals.[16] The spin-adapted open-shell singlet state is then obtained as twice the open-shell singlet minus the triplet. These methods provide result within chemical accuracy and remain remarkably stable across various density functionals from the classic PBE0-D4 (mean unsigned error, MUE: 0.029 eV) to the state-of-the-art optimally tuned (OT) range-separated hybrid (RSH) functional OT-ωB97M-V (MUE: 0.021 eV). In stark contrast, some of us showed in a recent paper[17] that the accuracy of time-dependent density functional theory (TD-DFT) in the Tamm-Dancoff approximation (TDA-DFT[18−20]) depends strongly on the chosen functional and solvation model. For most method combinations, outliers dominate the results, leading to deviations frequently exceeding the absolute ΔE_{ST} values. Only functionals with a small fraction of Fock exchange (≈10%), applied in vertical approximation (i.e., using ground-state structures) and evaluated without a proper solvent model, approach the accuracy of ΔDFT/PCM (MUE: 0.042 eV), which we attributed to strong error-cancellation effects. Accordingly, the good performance of this approach comes at the expense of overly stabilized CT states, sometimes by up to 1 eV, reminiscent of the CT failure of pure (meta-)GGA functionals.[21,22] To better identify such unreliable error-compensation-based methods and improve the diversity of the STGABS27 benchmark, we decided to include experimental emission energies E_{em}, which probe the energy difference between the polar excited CT (S_1) and the nonpolar ground state (GS). As such, emission energies offer a complementary challenge to the energy difference between two similar CT states (S_1 and T_1) in the original set, in which error-cancellation effects are much less helpful.

Countless previous studies have explored theoretical methods for calculating transition energies from and to CT excited states. For the sake of conciseness, we limit the following discussion to the most relevant ones. Shee and Head-Gordon recently investigated TD-DFT with a perturbative (pt)SS-PCM solvation model for the absorption and emission energies of twisted intramolecular (TI)CT excited states, including some TADF emitters.[23] They found optimally tuned RSH functionals such as OT-LC-ωPBE perform particularly well. Nonetheless, limitations of single-excitation-based TD-DFT persist, especially for smaller systems, which they attribute to missing orbital relaxation. Although they demonstrated that state-specific ΔROKS mitigates these errors, their approach lacked a proper account for solvation (they were taken from the TD-DFT calculations). A series of benchmarks by Jacquemin et al. on realistically sized organic emitters underscores the advantages of (OT-)RSH functionals.[24−28] Moreover, they emphasize the critical role of a state-specific nonequilibrium solvation model for treating CT states accurately. In another work, Jacquemin et al. explored the influence of correlation within a set of theoretical reference data for 30 intramolecular CT transitions.[29] Unfortunately, the prohibitive computational cost of high-level calculations limited the system size to only the smallest CT systems, in which orbital relaxation and dielectric stabilization are less important. While an RSH functional (ωB97X-D[30]) is again the most accurate with pure TD-DFT, more sophisticated wave function-based methods such as second-order algebraic diagrammatic construction ADC(2)[31,32] or second-order approximate coupled cluster CC2[33] provide some improvements. These findings were recently corroborated by Mester and Kállay,[34] further suggesting a benefit from an accurate explicit description of orbital relaxation. In this work, we want to systematically expand the benchmarking of CT emission energies in solution to ΔDFT-based methods, including a complete nonequilibrium solvation model. To this end, we implemented nonequilibrium state-specific solvation for ΔDFT in the Q-Chem program.[35]

This work adheres to the following structure: In section II, we present the reference values for the expansion of the STGABS27 set. Sections III and IV outline the theory and technical details necessary for calculating vertical emission energies with TDA-DFT and ΔDFT. Lastly, in section V, we illustrate the specific emission energies and the statistical performance of various density functionals on the expanded STGABS27 set to derive general recommendations for treating solvated CT states.

II. BENCHMARK SET

To thoroughly judge the applicability of an excited-state method for the CT states of TADF emitters, we extended the STGABS27 benchmark set with experimental emission energies E_{em} for all included systems. This new benchmark set shall be named STGABS27-EMS. Table 1 summarizes the key data, including reference emission energies, experimental measurement conditions, and corresponding literature references.

In contrast to the singlet−triplet gaps in STGABS27, where careful consideration of the experimental method was crucial to ensure reliable data for the mostly tiny energy differences < 0.1 eV, the 10−20 times larger emission energies can be taken from standard fluorescence spectra reported in the original publications. We primarily rely on the peak maximum or photoluminescence wavelength λ_{PL}. Where λ_{PL} was not explicitly stated (molecules 4, 12, 20, 22, and 25), we extracted the maximum position from the reported fluorescence spectra. Since polar CT states present in all but the multiple resonance (MR)-TADF emitters DABNA-1 (27) and DABNA-2 (26) exhibit a large bandwidth for the fluorescence peaks, we assume a statistical uncertainty in the emission energy of up to 10 nm (0.02−0.06 eV in the spectral region between 440−750 nm).

Further, we want to acknowledge that the fluorescence maximum typically does not directly correspond to the vertical emission energy at the optimized excited-state geometry. Discrepancies arise from differences in zero-point vibrational energy (ZPVE) between ground and excited state or vibrational effects leading to deviations from strictly vertical transitions.[24,61] Unfortunately, the strong S_1 CT character prevents a more well-founded comparison to 0−0 transitions, as the required absorption peak is typically weak and broad.[62] Moreover, 0−0 transitions, i.e., equilibrium-to-equilibrium, are not suitable for testing nonequilibrium solvation corrections for state-specific ΔDFT, which is a side goal of this work. Thus, we will compare E_{em} to the fluorescence maximum, arguing that this still provides valuable insights since most donor−acceptor type TADF emitters are rather similar regarding their electronic and chemical structure, which should lead to rather systematic deviations. Facing the same issue, other authors assume an uncertainty of absolute vertical emission energies ranging between 0.1 and 0.2 eV, of which we chose the latter as a conservative estimate.[23,24,61,63,64]

https://doi.org/10.1021/acs.jpca.4c03273
J. Phys. Chem. A 2024, 128, 6324−6335

Table 1. Names, Measurement Conditions, Experimental E_{em} Value (in eV), and Literature References for All Emitters of the STGABS27-EMS Set

no.	name	solvent[a]	E_{em}[h]	ref
1	MCz-XT	5 wt %: PPF[b]	2.59	36
2	TMCz-BO	10 μmol, tol.[c]	2.78	37
3	FAc-XT	5 wt %: PPF	2.54	36
4	PTZ-DBTO2	dilute tol.	2.12	38
5	ACRXTN	5 mol %: mCP[d]	2.59	39
6	PHOX-$^{Me}\pi$	20 μmol, tol.	1.99	40
7	PXZ-Mes_3B	10 μmol, tol.	2.44	41
8	TPA-PH2CN	10 μmol, tol.	2.52	42
9	oTE-DRZ	10 μmol, tol.	2.35	43
10	DACT-II	6 wt %: CBP[e]	2.40	44
11	XAc-XT	5 wt %: PPF	2.58	36
12	5Cz-TRZ	dilute tol.	2.48	45
13	2DAC-MES_3B	10 μmol, tol.	2.51	41
14	MFAc-OPS	10 μmol, tol.	2.80	46
15	MFAc-SPS	10 μmol, tol.	2.73	46
16	p-AC-DBNA	10 μmol, DCM[f]	2.23	47
17	3ACR-TRZ	10 μmol, tol.	2.43	48
18	m'-AC-DBNA	10 μmol, DCM	2.18	47
19	TPA-cNDI	10 μmol, tol.	1.65	49
20	4CzIPN	10 μmol, tol.	2.45	50
21	3DPA3CN	tol.	2.45	51
22	5CzBN	10 μmol, tol.	2.64	50
23	p-2Cz2BMe	10 μmol, tol.	2.22	52
24	ACRFLCN	6 wt %: TPSi-F[g]	2.56	53
25	Spiro-CN	6 wt %: mCP	2.30	54
26	DABNA-2	20 μmol, DCM	2.64	55
27	DABNA-1	20 μmol, DCM	2.68	56

[a]If no value for n^2 is known, 2.25 (toluene)[57] is used. [b]2,8-Bis(diphenylphosphoryl)dibenzo[b,d]furan: ε = 5.0.[58] [c]Toluene: ε = 2.37, n^2 = 2.25. [d]*N*,*N*′-Dicarbazolyl-3,5-benzene: ε = 2.84.[59] [e]4,4′-Bis(carbazol-9-yl)biphenyl: ε = 3.5 (see SI). [f]Dicholoromethane: ε = 8.93, n^2 = 2.03.[57] [g]Triphenyl-(4-(9-phenyl-9H-fluoren-9-yl)phenyl)-silane: ε = 2.5.[60] [h]Estimated accuracy ±0.02−0.06 eV in the given spectral region.

III. THEORY: SOLVATION FOR VERTICAL TRANSITIONS

In the following, we briefly introduce the theoretical background for calculating vertical transition energies in the presence of a dielectric continuum. We omit a comprehensive review of the underlying theory for polarizable continuum models (PCM) and instead refer the reader to relevant literature.[15,65−71] Throughout, we follow the notation established in ref 15, where a reaction field operator $\hat{R}_i$ of state $|\Psi_i\rangle$ polarizes the continuum and leads to the following state-specific Schrödinger equation

$$(\hat{H}^{vac} + \hat{R}_i)|\Psi_i\rangle = E_i|\Psi_i\rangle \quad (1)$$

Since electronic transitions occur on a much shorter time scale than the structural relaxation of the solute, the polarization response to the transition can be split into two parts, which can be regarded as the application of the Franck−Condon principle to the solvent: On the one hand, there is a fast electronic response from the solvent electronic degrees of freedom (DOF) that can follow the changing charge distribution of the solute, and on the other a slow orientational and vibrational response of the solvent nuclear DOFs, which remain unchanged. Therefore, we need to partition the total reaction field ($\propto \varepsilon$) into a fast part ($\propto \varepsilon_\infty = n^2$, with the refractive index n), and a remaining slow part[72−76]

$$\hat{R} = \hat{R}^f + \hat{R}^s \quad (2)$$

Accordingly, during a vertical transition from the equilibrium initial state fulfilling eq 1 (e.g., some excited state for emission) to the nonequilibrium final state, only the fast component $\hat{R}^f$ relaxes. Consequently, the Hamiltonian of the final state depends on both the fast component of its own and the slow component of the initial reaction field

$$\hat{H}_{final} = \hat{H}^{vac} + \hat{R}^f_{final} + \hat{R}^s_{initial} \quad (3)$$

The energy difference between the initial and final states defines the vertical emission energy E_{em}.

However, the strict application of this scheme results in a computationally demanding iterative approach and non-orthogonal states. To sidestep such complications, we avoid the interdependence between the initial and final states in the Hamiltonian by approximating the relaxation of $\hat{R}^f$ for the final state by perturbation theory (denoted ptSS-PCM,[69] closely related to the corrected linear-response (cLR)-PCM[77]), using the usual perturbation expression

$$\hat{R}^f_{final} = \hat{R}^f_{initial} + \lambda(\hat{R}^f_{final} - \hat{R}^f_{initial}) \quad (4)$$

The clear advantage of the perturbative approach is that the first-order perturbative approximation of the fast response of the final state (E^{1st}_{em}, compare Figure 1), can be obtained in a single step once the excited-state density is known.

Excitation- and ΔSCF-Based Procedures. Below, we detail the calculation of the initial excited and the final ground state with excitation- and ΔSCF-based methods, now integrated into the latest version of the Q-Chem program.[35]

In the state-specific (SS-)PCM formalism for excitation-based methods,[66,67,70,77−84] such as configuration interaction (CI[85]), algebraic diagrammatic construction (ADC(n)[31,32]), equation-of-motion/linear-response coupled cluster (EOM/LR-CC[86,87]), or TD(A)-DFT, the reaction field enters the calculation through the "solvated" ground-state orbitals. Consequently, to equilibrate the initial excited state, its reaction field has to be coupled back into the ground-state SCF. This is done in a procedure known as PerTurbation of Energy and Density (PTED) SS-PCM, illustrated on the left of Figure 1.[70] It begins with a ground-state SCF calculation, usually including a PCM (A) to produce initial orbitals for the excited-state TD-DFT calculation (B). From the TD-DFT calculation, we obtain the excited-state density used subsequently to polarize the continuum and yield the excited-state reaction field (C). This reaction field enters unchanged (frozen reaction field) into the next ground-state SCF (D), which produces an updated set of orbitals to return to step (B). Hence, at the high computational cost of repeated (iterative) calculation of the excited states, the PTED approach prepares both ground and excited states in the reaction field of the targeted excited state. Combined with the perturbative nonequilibrium approach described above (E), this allows the direct calculation of vertical emission energies.

For ΔSCF-based methods, the procedure depicted on the right of Figure 1 is more straightforward than for excitation-based methods, which originates in the state-specific nature of the ΔSCF approach: The inherent separation of the ground- and excited-state calculations in two distinct SCFs enables the concurrent optimization of the excited-state reaction field and

https://doi.org/10.1021/acs.jpca.4c03273
J. Phys. Chem. A 2024, 128, 6324−6335

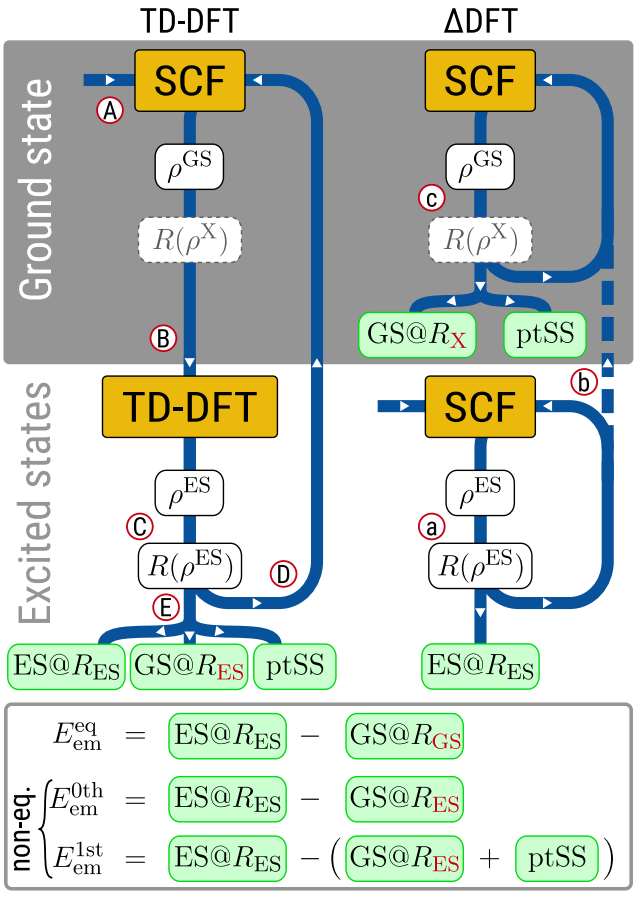

Figure 1. Schematic overview for the calculation of emission energies with either TD-DFT (left) or ΔDFT (right) in solution. White boxes indicate intermediates (the dashed $R(\rho^x)$ is replaced after the first iteration by the frozen excited-state reaction field of the excited state), while green boxes indicate final results. Letters A–E in the TD-DFT and letters a–c in the ΔDFT procedure mark steps that are referenced in the text.

the excited-state density (a), i.e., without the need to repeat the entire ground- and excited-state computation until convergence. Since isolated calculations yield each state under equilibrium conditions, the converged reaction field of the initial excited state must enter the final ground state (b). Ultimately, only a single SCF in this frozen reaction field is necessary (c) for the final ground state and the ptSS-PCM correction.

Let us finish with a few words about the nomenclature used in the following:

- ptSS-PCM always refers to the first-order corrected nonequilibrium transition energy. In the case of absorption, this means the ground-state equilibrated PCM and a ptSS-PCM term for relaxation in the excited state, and, in the case of emission, it means the excited-state equilibrated PCM and a ptSS-PCM term for relaxation to the ground state (E_{em}^{1st} in Figure 1).
- SS-PCM refers to fully equilibrated state energies, i.e., the lack of any ptSS nonequilibrium corrections (E_{em}^{eq}). For this, excitation-based methods require an iterative solvent-field optimization for each state (left of Figure 1), whereas full equilibration is the "natural" result in state-specific ΔDFT approaches. This would be the physically correct model for 0–0 transitions.
- Just "PCM" refers to calculations using the ground-state reaction field, i.e., no excited states are considered for solvation (correct for absorption at zeroth-order, E_{abs}^{0th}). This is the "natural" result of excitation-based approaches (when using solvated orbitals), while it does not naturally occur in ΔDFT approaches. Even though such ground-state solvation is incorrect for emission calculations (TDA-DFT calculation for the excited-state structure), it is the default solvation procedure in some quantum chemistry programs.
- Finally, the linear-response (LR-)PCM[88] is the default solvation model for TD-DFT in many programs also for excited-state optimizations, since analytical gradients may be available. As known for a long time, however, LR-PCM fails to recover the strong polarization response of CT states (see below).[69,89−91]
- Correct conditions for an emission calculation with the reaction field fixed to the excited state (E_{em}^{0th}) require an SS-PCM calculation only for the initial state, termed $SS^{initial}$-PCM. While excitation-based methods with SS-PCM naturally yield the final ground state in the reaction field of the initial excited state, ΔDFT requires a specific frozen reaction field SCF.

IV. COMPUTATIONAL DETAILS

All calculations were performed with a development version of the Q-Chem 5.4.2 program, containing the solvation model developments for TD(A)-DFT and ΔDFT described in section III. Emission energies were generally calculated in the vertical approximation at the relaxed structure of the first excited singlet state S_1, optimized at the same level of the theory. Since the state-specific PCM formalism for TDA-DFT lacks analytical nuclear gradients, geometry optimizations were carried out with TDA-DFT in the gas phase. Aside from exploratory calculations, all emission energies were calculated with state-specific PCM solvation with nonequilibrium effects added perturbatively via the ptSS-PCM (vide supra). The reaction field was divided into fast and slow components according to the Marcus partition,[92,93] with the required parameters ε and n for each solvent taken from the Minnesota Solvent Descriptor Database.[57]

Our selection of density functional approximations (DFAs) covers a range of global and optimally tuned[94,95] range-separated hybrid functionals mostly based on PBE.[96] For the global hybrids, the fraction a_x of admixed exact exchange varies between 10% for PBE10, 25% for PBE0,[97,37] and 37.5% for PBE38.[98] By interpreting a_x as a screening of electron–hole attraction in TDA-DFT calculations ($a_x = 1/\varepsilon$),[99−101] these admixtures equate to dielectric screening factors between ε = 10 (10%) and 2.6 (37.5%). For the range-separated hybrid functionals, we selected the optimally tuned LC-ωPBE (OT-LC-ωPBE, with no short-range Fock exchange)[102] and LRC-ωPBEh (OT-LRC-ωPBEh, 20% short-range Fock exchange)[103] as well as the best performer for singlet–triplet gaps on the STGABS27 set, the optimally tuned ωB97M-V (OT-ωB97M-V, 15% short-range Fock exchange)[104] functional. We omit untuned RSH functionals, as extensive prior studies found that the standard ω values, typically optimized for ground-state thermochemistry, are too large for excited-state applications.[1,23,26] The optimally tuned range-separation parameters ω were taken from ref 1. All calculations employ the DFT-D4 dispersion correction,[105,106] using the same

https://doi.org/10.1021/acs.jpca.4c03273
J. Phys. Chem. A 2024, 128, 6324−6335

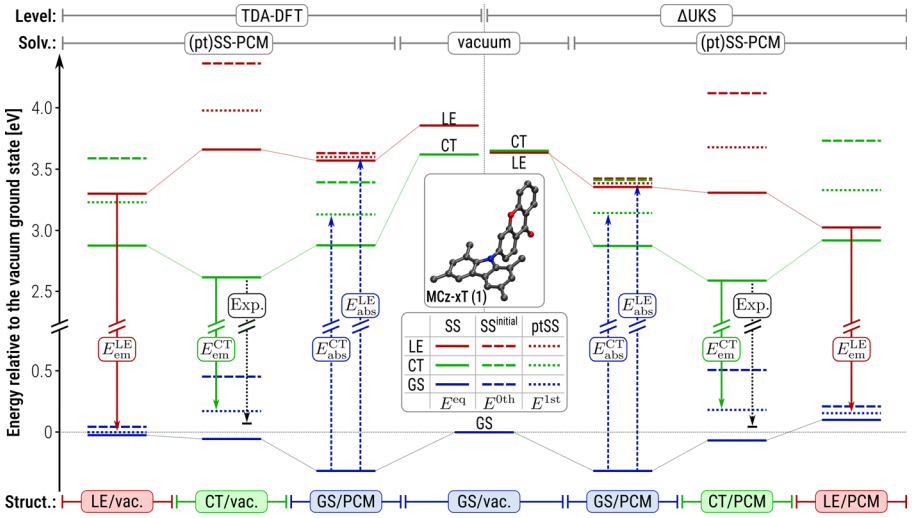

Figure 2. Energy level diagram for the TDA-DFT (left) and ΔUKS (right) calculation of absorption (dashed arrows) and emission energies (solid arrows) for the lowest charge-transfer (CT, green) and locally excited (LE, red) states of MCz-XT (molecule 1) solvated in a PPF matrix (ε = 5.00, n^2 = 2.25). All calculations employ the OT-ωB97M-V functional. For each possible initial state [ground state (GS, blue), CT, and LE], geometries indicated at the bottom are optimized (for TDA-DFT without solvation due to the lack of analytical nuclear gradients for SS-PCM). At each geometry, all states are calculated under equilibrium solvation conditions (SS-PCM, solid levels), in the reaction field of the initial state ($SS^{initial}$-PCM, dashed levels), and under first-order nonequilibrium conditions (ptSS-PCM, dotted levels). For comparison, the experimental emission energies are drawn in black.

damping parameters for OT-RSHs as in the untuned functional.[107] Furthermore, all calculations employ the def2-SVP basis set[108,109] (see the Supporting Information for a detailed basis set study).

V. RESULTS AND DISCUSSION

The Example of MCz-XT. Let us begin with an in-depth comparison of solvation effects at either the TDA-DFT or ΔDFT level, using 1,3,6,8-tetramethylcarbazole-xanthone (MCz-XT, molecule 1) as an example. Figure 2 shows the energy shifts caused by the dielectric environment for the ground (GS, blue), as well as the lowest CT (green) and LE (red) excited states of MCz-XT. Starting with MCz-XT in vacuum at the ground-state geometry (middle), both TDA-DFT and ΔUKS predict the CT and LE at around 3.7 eV, but with different ordering. TDA-DFT favors the CT state, while ΔUKS predicts a near degeneracy. For donor−acceptor TADF emitters containing extended π-systems, such as MCz-XT, near degeneracies between low-lying CT and LE states are common. Upon structural relaxation, either the CT or LE state can become the lowest one.

If we now include the dielectric environment, three distinct scenarios have to be considered, depending on the choice of the state for geometry optimization: (i) vertical absorption at the relaxed ground-state structure, as well as vertical emission at either (ii) the CT or (iii) LE excited-state structure. Let us begin with the optimized ground-state structure (i). Under equilibrium solvation conditions for each state (SS-PCM, solid levels), we find a consistent stabilization for all states with respect to the vacuum. The effect is more pronounced for the polar CT state (−0.69 or −0.86 eV) than in the less polar GS and LE state (−0.26 to −0.35 eV). Consequently, the CT state is invariably the lowest excited state. However, this is not as unambiguous under nonequilibrium conditions appropriate for modeling vertical absorption. Without any relaxation of the final excited-state reaction field (zeroth-order neq., $SS^{initial}$, dashed levels), the relative excited-state levels remain almost unchanged compared to the vacuum. In particular, the CT state experiences no special stabilization since the nonpolar GS only weakly polarizes the dielectric environment. Only the relaxation of the fast solvent DOFs to the specific excited state via the ptSS-PCM (first-order neq., dotted levels) drives the CT below the LE states and yields lower CT absorption energies ($E_{abs}^{1st,CT} < E_{abs}^{1st,LE}$). While the CT remains equal for TDA-DFT and ΔDFT, the absorption energies to the LE still reflect the initial gas phase energy discrepancy.

Moving on to the excited-state structures of CT (ii) and LE (iii), we identify two main factors for the vertical emission energies of either state at its optimal geometry, namely, (a) the overall stabilization due to the dielectric environment, and (b) the nonequilibrium effect on the ground state. For factor (a), we begin again with equilibrium solvation conditions. Compared to the ground-state structure, both states experience an additional energy lowering after state-specific geometry optimization. This seems to be dominated by the geometric relaxation of the solute as both CT and LE states respond similarly (≈0.25−0.3 eV, with either TDA-DFT or ΔUKS).

As for vertical absorption, nonequilibrium solvation (b) plays a crucial role for E_{em}. Whereas nonequilibrium solvation effects increase vertical absorption energies, vertical emission energies are consistently decreased compared to treating all states in their respective equilibrium conditions. The polarized CT reaction field greatly destabilizes the nonpolar ground state (+0.4−0.6 eV for zeroth-order and +0.2−0.3 eV first-order solvation) while nonequilibrium effects for emission from the LE state are negligible (below 0.1 eV). This destabilization is mostly due to the polarization work, which amounts to half of the interaction energy of the initial state (here CT) with its self-induced polarization. Because the polar CT strongly polarizes the environment, the polarization work is large whereas the interaction with the nonpolar ground state is small. Together, this results in a pronounced destabilization of the GS.[70]

https://doi.org/10.1021/acs.jpca.4c03273
J. Phys. Chem. A 2024, 128, 6324−6335

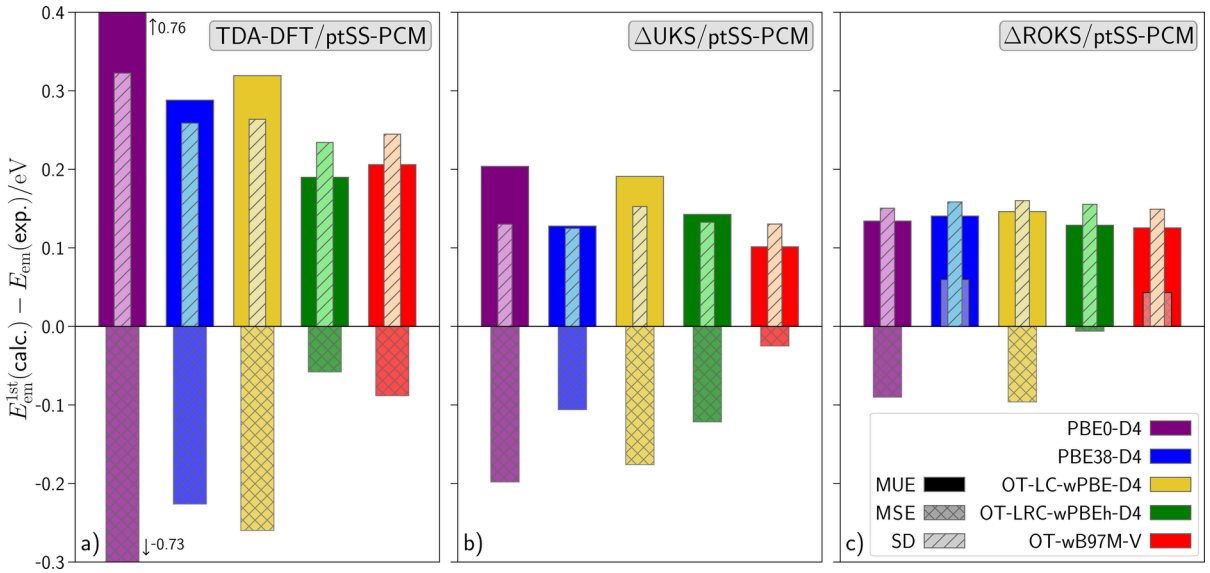

Figure 3. Plots of the MUE (solid outer bar), MSE (hatched middle bar), and SD (dashed inner bar) for the calculated E_{em}, relative to the experimental reference. Values are shown for different functionals at the (a) TDA-DFT/ptSS-PCM, (b) UKS/ptSS-PCM, and (c) ROKS/ptSS-PCM levels of theory. All calculations employ the S_1 optimized structures at the same level of theory (for TDA-DFT without solvation due to the lack of analytical nuclear gradients for SS-PCM).

Combined, the CT emission energy $E_{em}^{1st,CT}$ is lower than $E_{em}^{1st,LE}$ by 0.62 and 0.79 eV for TDA-DFT and ΔUKS, respectively, confirming the assignment of the experimental emission to the CT state. Again, the nonequilibrium solvation effects for TDA-DFT and ΔUKS occur largely in parallel, yielding very similar emission energies for the CT state (E_{em}^{CT} = 2.51 vs 2.48 eV). Both values agree excellently with the experiment (2.59 eV), especially when compared with the calculation in vacuum or the popular TDA-DFT/LR-PCM scheme (3.19 eV). These findings confirm that state-specific solvation, including appropriate nonequilibrium conditions for vertical transitions, cannot be neglected for either absorption or emission energies of competing low-energy CT and LE states.

TDA-DFT. Following our detailed analysis of MCz-XT, we continue with the statistical evaluation of the entire STGABS27-EMS benchmark set, beginning with the results for TDA-DFT. Figure 3a presents the statistical measures for TDA-DFT/ptSS-PCM with various density functionals. These statistics include the mean unsigned error (MUE), mean signed error (MSE), and standard deviation (SD); see the SI for definitions.

A striking initial observation is the strong functional dependence of E_{em}, which ranges from the promising accuracy of OT-LRC-ωPBEh-D4 (green) to a substantial underestimation with PBE0-D4 (purple, MSE ≈ − MUE = −0.73 eV). The crucial factor influencing performance is the fraction of nonlocal Fock exchange within the functional incorporated either globally (global hybrids) or in a distance-dependent way (range-separated hybrids). Increasing the global admixture, e.g., from 25% in PBE0-D4 to 37.5% in PBE38-D4 (blue), reduces the MUE by more than a factor of 2, primarily due to a decrease in the negative MSE accompanied by a minor reduction in SD. Among the optimally tuned RSHs, OT-LC-ωPBE-D4 (yellow, 0% short-range Fock exchange and 100% long-range Fock exchange) exhibits a similar error to PBE38-D4, while OT-LRC-ωPBEh-D4 (20% short-range and 100% long-range Fock exchange) and OT-ωB97M-V (red, 15% short-range and 100% long-range Fock exchange) are the most accurate. Interestingly, further analysis reveals a correlation between performance and Fock exchange fraction effective at the relevant electron−hole distance, as we already reported in a previous work.[17] For OT-LRC-ωPBEh, this fraction rises already around 0.7 Å above the 37.5% of PBE38-D4 compared to 1 Å for OT-LC-ωPBE (see Figure 2 in ref 17). To understand this curious trend of decreasing errors with increasing Fock exchange, we revisit our previous interpretation of the Fock exchange fraction as an effective dielectric screening between electron and hole ($\varepsilon \approx 1/a_x$, see ref 17 for details). Since the SS-PCM already accounts for screening due to the dielectric continuum, we suspect that only a limited further screening (large a_x) is required to mimic the effect of orbital relaxation. Notably, the opposite is true for predicting singlet−triplet gaps, where as little as 10% Fock exchange combined with an incomplete solvation model achieved the best performance with the help of a surprisingly stable error compensation.[17] This highlights the need for comprehensive testing across different properties to avoid methods that work primarily due to fortuitous error cancellation. In general, the observed performance of TDA-DFT/ptSS-PCM is in line with previous studies, which reported MUEs between 0.2 and 0.3 eV for the emission from CT states of similar emitters.[23,27,110] Notably, these studies also reported benefits from both system-specifically optimally tuned RSHs and increased fractions of Fock exchange.

ΔDFT. After exploring the accuracy of TDA-DFT, we now turn to the ΔDFT-based methods. Figure 3b and c illustrate the statistical analysis of the performance of ΔUKS/ptSS-PCM and ΔROKS/ptSS-PCM, respectively. From the start, it is clear that both are more consistent and provide much-improved emission energies as compared to TDA-DFT. Across all tested functionals, the MUE and the magnitude of the MSE are consistently below 0.2 eV, with the best-performing ΔUKS/OT-ωB97M-V achieving exceptional accuracy. Notably, this improved accuracy extends to the statistical error as measured by the SD, which is nearly halved compared to even the best

https://doi.org/10.1021/acs.jpca.4c03273
J. Phys. Chem. A 2024, 128, 6324−6335

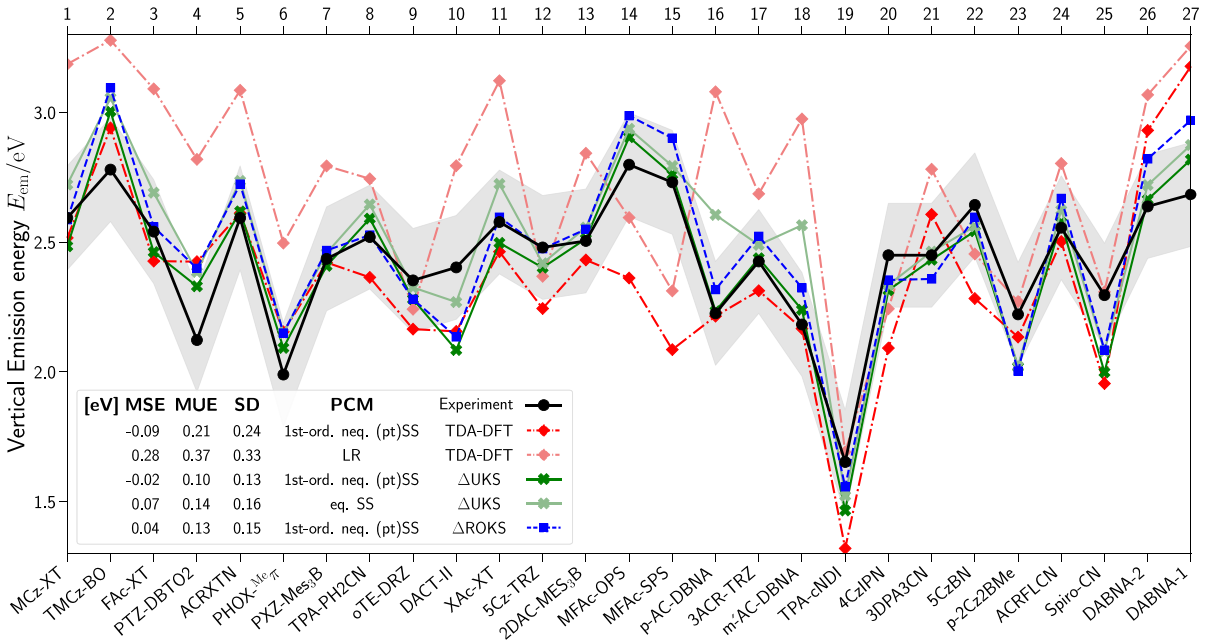

Figure 4. Experimental (black) and calculated emission energies E_{em} for the emitters of the STGABS27 benchmark set. The calculated values are given for the OT-ωB97M-V functionals with TDA-DFT (red, dash-dotted), ΔUKS (green, solid), and ΔROKS (blue, dashed) at the consistently optimized S_1 geometry. In addition to first-order nonequilibrium state-specific solvation conditions (ptSS-PCM, full colors), TDA-DFT/LR-PCM (shaded red) and ΔUKS/SS-PCM under equilibrium conditions (shaded green) are plotted. The parameters ε and n^2 were chosen for the measurement-specific solvent (see Table 1). An estimated uncertainty of ±0.2 eV for the experimental reference is marked by a gray band. MSE, MUE, and SD values for the set are tabulated.

TDA-DFT/SS-PCM method. This improvement of both systematic and statistical errors confirms that ΔDFT not only removes a systematic bias between experimental and calculated E_{em} values but leads to an overall more accurate description of the vertical emission process.

This improvement is clearly evident from the plot of the absolute emission energies (E_{em}) against the experimental references depicted in Figure 4 (see Supporting Information for plots including all tested methods). For OT-ωB97M-V, inspection shows that ΔDFT/ptSS-PCM (UKS in solid green, and ROKS in dashed blue lines) faithfully reproduces the relative trends in emission energies with only a few cases beyond the error range of 0.2 eV, whereas TDA-DFT/ptSS-PCM (red, dash-dotted line) exhibits much larger deviations and more than a third of the cases at or clearly outside the 0.2 eV range. Selected examples include systems 14 and 15, where TDA-DFT underestimates the emission energies by over 0.5 eV, or 20, 21, and 22, which reverse their relative order, and all of which are accurately described by the ΔDFT-based methods. While seemingly acceptable in a benchmark considering mostly statistical performance, it should be noted that such severe deviations for several of the studied molecules can critically deteriorate the performance of screening and optimization tasks in material design.[111,112] In this respect, having no outliers >0.3 eV is more important than eliminating small statistical deviations of ∼0.1 eV.

Furthermore, we want to emphasize the remarkable robustness of the ΔDFT approaches regarding functional choice. In particular, the SD shows minimal variation across different functionals, regardless of the amount of admixed Fock exchange. Apart from a rather systematic shift toward smaller emission energies (negative MSE), most functionals provide almost identical, highly accurate values for E_{em}. A remarkable example is the simple PBE38-D4 functional with ΔUKS/ptSS-PCM, which shows the lowest SD (0.13 eV) among all tested methods. This is particularly advantageous since it allows screening workflows without a sophisticated RSH or the computationally demanding system-specific optimal tuning procedure.

Having established the generally superior performance of time-independent ΔDFT/ptSS-PCM compared to the more common TD-DFT approach, we now turn to the choice of reference wave function for the open-shell singlet state. In other words, is the formally correct ROKS approach so much better than UKS that the additional computational cost is justified? Comparing the emission energies for UKS (green) and ROKS (blue) with OT-ωB97M-V in Figure 4, both curves run largely parallel to each other, with ROKS predicting slightly higher E_{em} values (between 0.07 and 0.17 eV increase in MSE). This systematic positive shift of ΔROKS (less negative MSE) holds for all tested functionals. We note that the singlet−triplet gap ΔE_{ST} displays a similar trend, where ROKS yields generally larger values than UKS due to a more destabilized singlet state.[113,114] The explanation lies in the inherent difference between UKS and ROKS wave functions. ROKS incorporates two determinants for proper spin-adaptation, avoiding the unwanted admixture of the energetically close but lower triplet state known as spin-contamination. Interestingly, the statistical measures suggest a slight benefit from the spin-contamination in UKS. This even extends to the statistical error (SD) indicating that UKS is more accurate despite its formally incorrect handling of open-shell singlets, at least for the CT states studied herein. Hence, since the additional effort for ROKS offers no improvement in accuracy, the more widely available ΔUKS should be used for generally accurate emission energies of CT states.

Solvation Models. After a detailed discussion of aspects of the electronic structure method applied to the solute, let us

https://doi.org/10.1021/acs.jpca.4c03273
J. Phys. Chem. A 2024, 128, 6324−6335

now examine the influence of the solvent model for the dielectric environment. Figure 5 shows the statistical measures

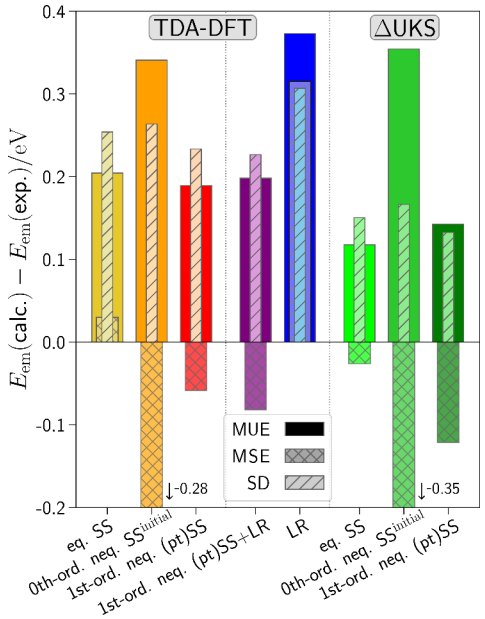

Figure 5. Plots of the MUE (solid outer bar), MSE (hatched middle bar), and SD (dashed inner bar) for the calculated E_{em} relative to the experimental reference. Values are shown for TDA-DFT and ΔUKS with different solvation models. All calculations use the OT-LRC-ωPBEh-D4 functional and S_1 optimized structures (for TDA-DFT without solvation).

for TDA-DFT and ΔUKS with the OT-LRC-ωPBEh-D4 functional and different excited-state solvation models. For TDA-DFT, there are several choices for the excited-state solvation model: In addition to the physically complete LR-PCM or (pt)SS-PCM models, one may use the ground-state PCM or SS-PCM without first-order ptSS-corrections ($SS^{initial}$). Here, we begin with TDA-DFT/SS-PCM under equilibrium conditions for ground and excited states (E_{em}^{eq}, yellow bar), which marginally overestimates the emission energies. However, nonequilibrium effects must be considered to account for the limited duration of the vertical emission process (see scheme in Figure 1). In the zeroth-order $SS^{initial}$ approach (E_{em}^{0th}, orange bar), which neglects any solvent relaxation upon emission, E_{em} is systematically overestimated (negative MSE), as we already saw in the exemplary case of MCz-XT (vide supra). Balanced emission energies require the relaxation of the fast electronic solvent DOFs at first-order via the ptSS-PCM correction (E_{em}^{1st}, red bar). Notably, the ptSS-PCM treatment also yields the lowest SD, which confirms the advantage of nonequilibrium solvation for vertical transitions. A similar trend emerges for the stepwise introduction of nonequilibrium solvation in the ΔUKS calculations, albeit at a substantially lower overall error (especially the SD). We can again compare the explicit emission energies predicted in the nonequilibrium (bright green) and equilibrium (shaded green) regimes displayed in Figure 4. Accounting for nonequilibrium solvation generally reduces the emission energies, though not uniformly by the same amount. The differences arise from the specific solvent used during measurement. Only polar solvents, where the total (ε) and infinite-frequency (ε_∞) dielectric constants deviate substantially, such as DCM or PPF (systems 1, 3, 11, 16, 18, 26, and 27), exhibit a significant nonequilibrium effect. Meanwhile, for nonpolar solvents dominated by fast polarization, such as toluene, equilibrium and nonequilibrium conditions deviate only negligibly.

Knowing that sophisticated nonequilibrium solvation with the SS-PCM model for TDA-DFT works well, we also investigated the more widely available and popular LR-PCM model. Benefits of LR-PCM compared to state-specific approaches include that the solvent response is treated for all states simultaneously, and analytical gradients are often available. However, a straightforward application of LR-PCM (blue bar) yields large errors stemming from a combined increase in the statistical error (larger SD) and a systematic overestimation of emission energies (positive MSE). This is also apparent from the E_{em} values plotted in Figure 4 (dash-dotted shaded red line). The substantial error arises from the near-zero contribution in the transition-density-based LR-PCM model, which is clearly a result of the vanishing transition density of polar CT states. Consequently, the simultaneous use of LR- and nonequilibrium SS-PCM, as suggested in ref 69, also changes the results only slightly. Therefore, we conclude that any treatment of CT states with excitation-based models should include SS-PCM solvation since LR-PCM fails to recover the large dielectric stabilization of such states.

VI. CONCLUSIONS

We presented an extension of the STGABS27 benchmark set for singlet−triplet gaps to experimental emission energies E_{em}, termed STGABS27-EMS. This new data complements the existing singlet−triplet gaps ΔE_{ST} for 27 TADF emitters, allowing a more robust test of excited-state methods. The combined benchmark data probes polar CT states not only relative to each other[1,17] but also relative to the nonpolar ground state, which allowed us to refine our recommendations for treating charge transfer states in solution. In particular, STGABS27-EMS enabled us to explore the nuances of functional choice and excited-state solvation for vertical transitions based on TDA-DFT and ΔDFT.

The primary result of this work is that ΔDFT/PCM-based approaches can predict emission energies of CT states of typical TADF emitters with higher accuracy and robustness than TDA-based approaches, as evident from the excellent mean unsigned errors of 0.10 eV and standard deviation of 0.13 eV for the best-performing OT-ωB97M-V with ΔUKS/ptSS-PCM. Such deviations fall within our assumed maximum uncertainty for the reference E_{em} values, suggesting our initial estimate of 0.2 eV might be too conservative. Moreover, the ΔDFT accuracy shows at least a four times smaller sensitivity to the functional choice than TDA-based approaches. Accordingly, the largest shift of the MSE between the tested functionals is 0.67 eV for TDA-DFT, whereas the respective shift is just 0.17/0.16 eV for UKS/ROKS. TDA-DFT introduces systematic shifts in the emission energies and the accuracy depends more on the functional. This is evident from the SD, which varies between 0.23 and 0.32 eV for TDA, while it remains below 0.15/0.16 eV with UKS/ROKS. Hence, TDA-DFT calculations for CT require state-of-art range-separated hybrids in combination with optimal tuning and the sophisticated ptSS-PCM solvation model, whereas a ΔDFT calculation can employ any reasonable hybrid DFA, as evident from the good performance UKS/PBE38-D4. Clearly, the newly implemented nonequilibrium ptSS-PCM solvation for ΔDFT further improves the vertical emission energies,

https://doi.org/10.1021/acs.jpca.4c03273
J. Phys. Chem. A 2024, 128, 6324−6335

highlighting the general need for proper state-specific solvation.

In stark contrast, the most widely used excited-state method, TD-DFT or TDA-DFT with SS-PCM solvation, exhibits much larger deviations even with the best-performing OT-LRC-ωPBEh-D4 functional (MUE: 0.19 eV, SD: 0.23 eV). Unlike in our prior studies of singlet−triplet gaps, where a minimal admixture of ∼10% Fock exchange yields optimal error cancelation, emission energies require a large fraction (>38%). Furthermore, we again confirmed the benefit of state-specific excited-state solvation, as the commonly employed LR-PCM variant yields only a negligible stabilization over the vacuum. Although the best TDA-DFT/ptSS-PCM approach provides reasonable errors below 0.2 eV, it is not generally reliable for CT states in TADF emitters.

In conclusion, the combined benchmarking of ΔE_{ST} and E_{em} strongly suggests that ΔDFT/PCM methods provide a generally robust and accurate account of polar CT states in solution. This success can be attributed to (i) the explicit account for orbital relaxation, (ii) an inherently state-specific treatment of solvation, and (iii) the avoidance of the long-range CT failure of TD-DFT.

■ ASSOCIATED CONTENT

Supporting Information

The Supporting Information is available free of charge at https://pubs.acs.org/doi/10.1021/acs.jpca.4c03273.

Detailed description of the computational workflow, methods, and used programs; complete plots of the emission energies for all used methods; investigation of basis set effects; definition of the used statistical measures (PDF)

All optimized geometries of both singlet and triplet states, as well as all used input and output files for the presented results (ZIP)

■ AUTHOR INFORMATION

Corresponding Author

Jan-Michael Mewes − *Mulliken Center for Theoretical Chemistry, University of Bonn, 53115 Bonn, Germany; beeOLED GmbH, 01257 Dresden, Germany;* orcid.org/0000-0002-4669-8091; Email: janmewes@janmewes.de

Authors

Thomas Froitzheim − *Mulliken Center for Theoretical Chemistry, University of Bonn, 53115 Bonn, Germany;* orcid.org/0000-0001-9853-0410

Lukas Kunze − *Mulliken Center for Theoretical Chemistry, University of Bonn, 53115 Bonn, Germany;* orcid.org/0000-0001-5605-5236

Stefan Grimme − *Mulliken Center for Theoretical Chemistry, University of Bonn, 53115 Bonn, Germany;* orcid.org/0000-0002-5844-4371

John M. Herbert − *Department of Chemistry and Biochemistry, The Ohio State University, Columbus, Ohio 43210, United States;* orcid.org/0000-0002-1663-2278

Complete contact information is available at: https://pubs.acs.org/10.1021/acs.jpca.4c03273

Author Contributions

‖These authors contributed equally

Notes

The authors declare the following competing financial interest(s): J.M.H. is part owner of Q-Chem and serves on its board of directors.

■ ACKNOWLEDGMENTS

T.F. acknowledges the Fonds der Chemischen Industrie (FCI) for funding under a Kekulé scholarship. This project has been funded with support from the RTG-2591 "TIDE-Template-designed Organic Electronics" by the DFG. J.M.H. was supported by the U.S. National Science Foundation, grant no. CHE-1955282.

■ REFERENCES

(1) Kunze, L.; Hansen, A.; Grimme, S.; Mewes, J. M. PCM-ROKS for the Description of Charge-Transfer States in Solution: Singlet-Triplet Gaps with Chemical Accuracy from Open-Shell Kohn-Sham Reaction-Field Calculations. *J. Phys. Chem. Lett.* **2021**, *12*, 8470−8480.

(2) Zhang, Q.; Li, B.; Huang, S.; Nomura, H.; Tanaka, H.; Adachi, C. Efficient blue organic light-emitting diodes employing thermally activated delayed fluorescence. *Nat. Photonics* **2014**, *8*, 326−332.

(3) Dias, F. B.; Penfold, T. J.; Monkman, A. P. Photophysics of thermally activated delayed fluorescence molecules. *Methods and Applications in Fluorescence* **2017**, *5*, 012001.

(4) Yang, Z.; Mao, Z.; Xie, Z.; Zhang, Y.; Liu, S.; Zhao, J.; Xu, J.; Chi, Z.; Aldred, M. P. Recent advances in organic thermally activated delayed fluorescence materials. *Chem. Soc. Rev.* **2017**, *46*, 915−1016.

(5) Wong, M. Y.; Zysman-Colman, E. Purely Organic Thermally Activated Delayed Fluorescence Materials for Organic Light-Emitting Diodes. *Adv. Mater.* **2017**, *29*, 1605444.

(6) Samanta, P. K.; Kim, D.; Coropceanu, V.; Brédas, J.-L. Up-Conversion Intersystem Crossing Rates in Organic Emitters for Thermally Activated Delayed Fluorescence: Impact of the Nature of Singlet vs Triplet Excited States. *J. Am. Chem. Soc.* **2017**, *139*, 4042−4051.

(7) Huang, T.; Jiang, W.; Duan, L. Recent progress in solution processable TADF materials for organic light-emitting diodes. *Journal of Materials Chemistry C* **2018**, *6*, 5577−5596.

(8) Mewes, J.-M. Modeling TADF in organic emitters requires a careful consideration of the environment and going beyond the Franck−Condon approximation. *Phys. Chem. Chem. Phys.* **2018**, *20*, 12454−12469.

(9) Berberan-Santos, M. N.; Garcia, J. M. M. Unusually Strong Delayed Fluorescence of C_{70}. *J. Am. Chem. Soc.* **1996**, *118*, 9391−9394.

(10) Frank, I.; Hutter, J.; Marx, D.; Parrinello, M. Molecular dynamics in low-spin excited states. *J. Chem. Phys.* **1998**, *108*, 4060−4069.

(11) Kowalczyk, T.; Tsuchimochi, T.; Chen, P.-T.; Top, L.; Van Voorhis, T. Excitation energies and Stokes shifts from a restricted open-shell Kohn-Sham approach. *J. Chem. Phys.* **2013**, *138*, 164101.

(12) Gilbert, A. T. B.; Besley, N. A.; Gill, P. M. W. Self-Consistent Field Calculations of Excited States Using the Maximum Overlap Method (MOM). *J. Phys. Chem. A* **2008**, *112*, 13164−13171.

(13) Barca, G. M. J.; Gilbert, A. T. B.; Gill, P. M. W. Simple Models for Difficult Electronic Excitations. *J. Chem. Theory Comput.* **2018**, *14*, 1501−1509.

(14) Miertuš, S.; Scrocco, E.; Tomasi, J. Electrostatic interaction of a solute with a continuum. A direct utilizaion of ab initio molecular potentials for the prevision of solvent effects. *Chem. Phys.* **1981**, *55*, 117−129.

(15) Herbert, J. M. Dielectric continuum methods for quantum chemistry. *Wiley Interdisciplinary Reviews: Computational Molecular Science* **2021**, *11*, No. e1519.

(16) Hait, D.; Head-Gordon, M. Orbital Optimized Density Functional Theory for Electronic Excited States. *J. Phys. Chem. Lett.* **2021**, *12*, 4517−4529.
(17) Froitzheim, T.; Grimme, S.; Mewes, J.-M. Either Accurate Singlet−Triplet Gaps or Excited-State Structures: Testing and Understanding the Performance of TD-DFT for TADF Emitters. *J. Chem. Theory Comput.* **2022**, *18*, 7702−7713.
(18) Runge, E.; Gross, E. K. U. Density-Functional Theory for Time-Dependent Systems. *Phys. Rev. Lett.* **1984**, *52*, 997−1000.
(19) Petersilka, M.; Gossmann, U. J.; Gross, E. K. U. Excitation Energies from Time-Dependent Density-Functional Theory. *Phys. Rev. Lett.* **1996**, *76*, 1212−1215.
(20) Hirata, S.; Head-Gordon, M. Time-dependent density functional theory within the Tamm−Dancoff approximation. *Chem. Phys. Lett.* **1999**, *314*, 291−299.
(21) Dreuw, A.; Head-Gordon, M. Failure of Time-Dependent Density Functional Theory for Long-Range Charge-Transfer Excited States: The Zincbacteriochlorin-Bacteriochlorin and Bacteriochlorophyll-Spheroidene Complexes. *J. Am. Chem. Soc.* **2004**, *126*, 4007−4016.
(22) Dreuw, A.; Head-Gordon, M. Single-Reference ab Initio Methods for the Calculation of Excited States of Large Molecules. *Chem. Rev.* **2005**, *105*, 4009−4037.
(23) Shee, J.; Head-Gordon, M. Predicting Excitation Energies of Twisted Intramolecular Charge-Transfer States with the Time-Dependent Density Functional Theory: Comparison with Experimental Measurements in the Gas Phase and Solvents Ranging from Hexanes to Acetonitrile. *J. Chem. Theory Comput.* **2020**, *16*, 6244−6255.
(24) Jacquemin, D.; Wathelet, V.; Perpète, E. A.; Adamo, C. Extensive TD-DFT Benchmark: Singlet-Excited States of Organic Molecules. *J. Chem. Theory Comput.* **2009**, *5*, 2420−2435.
(25) Jacquemin, D.; Planchat, A.; Adamo, C.; Mennucci, B. TD-DFT Assessment of Functionals for Optical 0−0 Transitions in Solvated Dyes. *J. Chem. Theory Comput.* **2012**, *8*, 2359−2372.
(26) Jacquemin, D.; Moore, B. I.; Planchat, A.; Adamo, C.; Autschbach, J. Performance of an Optimally Tuned Range-Separated Hybrid Functional for 0−0 Electronic Excitation Energies. *J. Chem. Theory Comput.* **2014**, *10*, 1677−1685.
(27) Jacquemin, D.; Duchemin, I.; Blase, X. 0−0 Energies Using Hybrid Schemes: Benchmarks of TD-DFT, CIS(D), ADC(2), CC2, and BSE/GW formalisms for 80 Real-Life Compounds. *J. Chem. Theory Comput.* **2015**, *11*, 5340−5359.
(28) Budzak, S.; Jaunet-Lahary, T.; Laurent, A. D.; Laurence, C.; Medved, M.; Jacquemin, D. Exploring the Solvatochromism of Betaine 30 with Ab Initio Tools: From Accurate Gas-Phase Calculations to Implicit and Explicit Solvation Models. *Chemistry − A European Journal* **2017**, *23*, 4108−4119.
(29) Loos, P.-F.; Comin, M.; Blase, X.; Jacquemin, D. Reference Energies for Intramolecular Charge-Transfer Excitations. *J. Chem. Theory Comput.* **2021**, *17*, 3666−3686.
(30) Chai, J.-D.; Head-Gordon, M. Long-range corrected hybrid density functionals with damped atom−atom dispersion corrections. *Phys. Chem. Chem. Phys.* **2008**, *10*, 6615−6620.
(31) Schirmer, J. Beyond the random-phase approximation: A new approximation scheme for the polarization propagator. *Phys. Rev. A* **1982**, *26*, 2395−2416.
(32) Trofimov, A. B.; Schirmer, J. An efficient polarization propagator approach to valence electron excitation spectra. *Journal of Physics B: Atomic, Molecular and Optical Physics* **1995**, *28*, 2299.
(33) Christiansen, O.; Koch, H.; Jørgensen, P. The second-order approximate coupled cluster singles and doubles model CC2. *Chem. Phys. Lett.* **1995**, *243*, 409−418.
(34) Mester, D.; Kállay, M. Charge-Transfer Excitations within Density Functional Theory: How Accurate Are the Most Recommended Approaches? *J. Chem. Theory Comput.* **2022**, *18*, 1646−1662.
(35) Epifanovsky, E.; et al. Software for the frontiers of quantum chemistry: An overview of developments in the Q-Chem 5 package. *J. Chem. Phys.* **2021**, *155*, 084801.
(36) Lee, J.; Aizawa, N.; Numata, M.; Adachi, C.; Yasuda, T. Versatile Molecular Functionalization for Inhibiting Concentration Quenching of Thermally Activated Delayed Fluorescence. *Adv. Mater.* **2017**, *29*, 1604856.
(37) Kim, J. U.; Park, I. S.; Chan, C.-Y.; Tanaka, M.; Tsuchiya, Y.; Nakanotani, H.; Adachi, C. Nanosecond-time-scale delayed fluorescence molecule for deep-blue OLEDs with small efficiency rolloff. *Nat. Commun.* **2020**, *11*, 1765.
(38) Nobuyasu, R. S.; Ren, Z.; Griffiths, G. C.; Batsanov, A. S.; Data, P.; Yan, S.; Monkman, A. P.; Bryce, M. R.; Dias, F. B. Rational Design of TADF Polymers Using a Donor−Acceptor Monomer with Enhanced TADF Efficiency Induced by the Energy Alignment of Charge Transfer and Local Triplet Excited States. *Advanced Optical Materials* **2016**, *4*, 597−607.
(39) Inoue, M.; Serevilius, T.; Nakanotani, H.; Yoshida, K.; Matsushima, T.; Jurslnas, S.; Adachi, C. Effect of reverse intersystem crossing rate to suppress efficiency roll-off in organic light-emitting diodes with thermally activated delayed fluorescence emitters. *Chem. Phys. Lett.* **2016**, *644*, 62−67.
(40) Narsaria, A. K.; et al. Computationally Guided Molecular Design to Minimize the LE/CT Gap in D-π-A Fluorinated Triarylboranes for Efficient TADF via D and π-Bridge Tuning. *Adv. Funct. Mater.* **2020**, *30*, 2002064.
(41) Suzuki, K.; Kubo, S.; Shizu, K.; Fukushima, T.; Wakamiya, A.; Murata, Y.; Adachi, C.; Kaji, H. Triarylboron-Based Fluorescent Organic Light-Emitting Diodes with External Quantum Efficiencies Exceeding 20%. *Angew. Chem., Int. Ed.* **2015**, *54*, 15231−15235.
(42) Sommer, G. A.; Mataranga-Popa, L. N.; Czerwieniec, R.; Hofbeck, T.; Homeier, H. H. H.; Müller, T. J. J.; Yersin, H. Design of Conformationally Distorted Donor−Acceptor Dyads Showing Efficient Thermally Activated Delayed Fluorescence. *J. Phys. Chem. Lett.* **2018**, *9*, 3692−3697.
(43) Cai, X.; Qiao, Z.; Li, M.; Wu, X.; He, Y.; Jiang, X.; Cao, Y.; Su, S.-J. Purely Organic Crystals Exhibit Bright Thermally Activated Delayed Fluorescence. *Angew. Chem.* **2019**, *131*, 13656−13665.
(44) Kaji, H.; et al. Purely organic electroluminescent material realizing 100% conversion from electricity to light. *Nat. Commun.* **2015**, *6*, 8476.
(45) Cui, L.-S.; et al. Fast spin-flip enables efficient and stable organic electroluminescence from charge-transfer states. *Nat. Photonics* **2020**, *14*, 636−642.
(46) Lee, J.; Aizawa, N.; Yasuda, T. Molecular engineering of phosphacycle-based thermally activated delayed fluorescence materials for deep-blue OLEDs. *Journal of Materials Chemistry C* **2018**, *6*, 3578−3583.
(47) Meng, G.; Chen, X.; Wang, X.; Wang, N.; Peng, T.; Wang, S. TADF Emitters: Isomeric Bright Sky-Blue TADF Emitters Based on Bisacridine Decorated DBNA: Impact of Donor Locations on Luminescent and Electroluminescent Properties. *Advanced Optical Materials* **2019**, *7*, 1900130.
(48) Wada, Y.; Shizu, K.; Kubo, S.; Suzuki, K.; Tanaka, H.; Adachi, C.; Kaji, H. Highly efficient electroluminescence from a solution-processable thermally activated delayed fluorescence emitter. *Appl. Phys. Lett.* **2015**, *107*, 183303.
(49) Higginbotham, H. F.; Pander, P.; Rybakiewicz, R.; Etherington, M. K.; Maniam, S.; Zagorska, M.; Pron, A.; Monkman, A. P.; Data, P. Triphenylamine disubstituted naphthalene diimide: elucidation of excited states involved in TADF and application in near-infrared organic light emitting diodes. *Journal of Materials Chemistry C* **2018**, *6*, 8219−8225.
(50) Noda, H.; Chen, X.-K.; Nakanotani, H.; Hosokai, T.; Miyajima, M.; Notsuka, N.; Kashima, Y.; Brédas, J.-L.; Adachi, C. Critical role of intermediate electronic states for spin-flip processes in charge-transfer-type organic molecules with multiple donors and acceptors. *Nat. Mater.* **2019**, *18*, 1084−1090.
(51) Taneda, M.; Shizu, K.; Tanaka, H.; Adachi, C. High efficiency thermally activated delayed fluorescence based on 1,3,5-tris(4-(diphenylamino)phenyl)-2,4,6-tricyanobenzene. *Chem. Commun.* **2015**, *51*, 5028−5031.

https://doi.org/10.1021/acs.jpca.4c03273
J. Phys. Chem. A 2024, 128, 6324−6335

(52) Noda, H.; Nakanotani, H.; Adachi, C. Highly Efficient Thermally Activated Delayed Fluorescence with Slow Reverse Intersystem Crossing. *Chem. Lett.* **2019**, *48*, 126−129.
(53) Méhes, G.; Nomura, H.; Zhang, Q.; Nakagawa, T.; Adachi, C. Enhanced Electroluminescence Efficiency in a Spiro-Acridine Derivative through Thermally Activated Delayed Fluorescence. *Angew. Chem., Int. Ed.* **2012**, *51*, 11311−11315.
(54) Nakagawa, T.; Ku, S.-Y.; Wong, K.-T.; Adachi, C. Electroluminescence based on thermally activated delayed fluorescence generated by a spirobifluorene donor−acceptor structure. *Chem. Commun.* **2012**, *48*, 9580−9582.
(55) Nakanotani, H.; Furukawa, T.; Hosokai, T.; Hatakeyama, T.; Adachi, C. Light Amplification in Molecules Exhibiting Thermally Activated Delayed Fluorescence. *Advanced Optical Materials* **2017**, *5*, 1700051.
(56) Hatakeyama, T.; Shiren, K.; Nakajima, K.; Nomura, S.; Nakatsuka, S.; Kinoshita, K.; Ni, J.; Ono, Y.; Ikuta, T. Ultrapure Blue Thermally Activated Delayed Fluorescence Molecules: Efficient HOMO−LUMO Separation by the Multiple Resonance Effect. *Adv. Mater.* **2016**, *28*, 2777−2781.
(57) Winget, P.; Dolney, D.; Giesen, D.; Cramer, C.; Truhlar, D. *Minnesota Solvent Descriptor Database*. https://comp.chem.umn.edu/solvation/mnsddb.pdf.
(58) Vecchi, P. A.; Padmaperuma, A. B.; Qiao, H.; Sapochak, L. S.; Burrows, P. E. A Dibenzofuran-Based Host Material for Blue Electrophosphorescence. *Org. Lett.* **2006**, *8*, 4211−4214.
(59) Skuodis, E.; Bezvikonnyi, O.; Tomkeviciene, A.; Volyniuk, D.; Mimaite, V.; Lazauskas, A.; Bucinskas, A.; Keruckiene, R.; Sini, G.; Grazulevicius, J. V. Aggregation, thermal annealing, and hosting effects on performances of an acridan-based TADF emitter. *Org. Electron.* **2018**, *63*, 29−40.
(60) Shih, P.-I.; Chien, C.-H.; Chuang, C.-Y.; Shu, C.-F.; Yang, C.-H.; Chen, J.-H.; Chi, Y. Novel host material for highly efficient blue phosphorescent OLEDs. *J. Mater. Chem.* **2007**, *17*, 1692−1698.
(61) Lasorne, B.; Jornet-Somoza, J.; Meyer, H.-D.; Lauvergnat, D.; Robb, M. A.; Gatti, F. Vertical transition energies vs. absorption maxima: Illustration with the UV absorption spectrum of ethylene. *Spectrochimica Acta Part A: Molecular and Biomolecular Spectroscopy* **2014**, *119*, 52−58.
(62) Tian, X.; Sun, H.; Zhang, Q.; Adachi, C. Theoretical predication for transition energies of thermally activated delayed fluorescence molecules. *Chin. Chem. Lett.* **2016**, *27*, 1445−1452.
(63) Adamo, C.; Jacquemin, D. The calculations of excited-state properties with Time-Dependent Density Functional Theory. *Chem. Soc. Rev.* **2013**, *42*, 845−856.
(64) Laurent, A. D.; Jacquemin, D. TD-DFT benchmarks: A review. *Int. J. Quantum Chem.* **2013**, *113*, 2019−2039.
(65) Tomasi, J.; Mennucci, B.; Cancès, E. The IEF version of the PCM solvation method: an overview of a new method addressed to study molecular solutes at the QM ab initio level. *Journal of Molecular Structure: THEOCHEM* **1999**, *464*, 211−226.
(66) Improta, R.; Barone, V.; Scalmani, G.; Frisch, M. J. A state-specific polarizable continuum model time dependent density functional theory method for excited state calculations in solution. *J. Chem. Phys.* **2006**, *125*, 054103.
(67) Improta, R.; Scalmani, G.; Frisch, M. J.; Barone, V. Toward effective and reliable fluorescence energies in solution by a new state specific polarizable continuum model time dependent density functional theory approach. *J. Chem. Phys.* **2007**, *127*, 074504.
(68) Marenich, A. V.; Cramer, C. J.; Truhlar, D. G.; Guido, C. A.; Mennucci, B.; Scalmani, G.; Frisch, M. J. Practical computation of electronic excitation in solution: Vertical excitation model. *Chemical Science* **2011**, *2*, 2143−2161.
(69) Mewes, J. M.; You, Z. Q.; Wormit, M.; Kriesche, T.; Herbert, J. M.; Dreuw, A. Experimental benchmark data and systematic evaluation of two a posteriori, polarizable-continuum corrections for vertical excitation energies in solution. *J. Phys. Chem. A* **2015**, *119*, 5446−5464.
(70) Mewes, J. M.; Herbert, J. M.; Dreuw, A. On the accuracy of the general, state-specific polarizable-continuum model for the description of correlated ground- and excited states in solution. *Phys. Chem. Chem. Phys.* **2017**, *19*, 1644−1654.
(71) Guido, C. A.; Caprasecca, S. On the description of the environment polarization response to electronic transitions. *Int. J. Quantum Chem.* **2019**, *119*, No. e25711.
(72) McRae, E. G. Theory of Solvent Effects on Molecular Electronic Spectra. Frequency Shifts. *J. Phys. Chem.* **1957**, *61*, 562−572.
(73) Lippert, E. Spektroskopische Bestimmung des Dipolmomentes aromatischer Verbindungen im ersten angeregten Singulettzustand. *Zeitschrift für Elektrochemie, Berichte der Bunsengesellschaft für physikalische Chemie* **1957**, *61*, 962−975.
(74) Brady, J. E.; Carr, P. W. An analysis of dielectric models of solvatochromism. *J. Phys. Chem.* **1985**, *89*, 5759−5766.
(75) Klamt, A. Calculation of UV/Vis Spectra in Solution. *J. Phys. Chem.* **1996**, *100*, 3349−3353.
(76) You, Z. Q.; Mewes, J. M.; Dreuw, A.; Herbert, J. M. Comparison of the Marcus and Pekar partitions in the context of non-equilibrium, polarizable-continuum solvation models. *J. Chem. Phys.* **2015**, *143*, 204104.
(77) Caricato, M.; Mennucci, B.; Tomasi, J.; Ingrosso, F.; Cammi, R.; Corni, S.; Scalmani, G. Formation and relaxation of excited states in solution: A new time dependent polarizable continuum model based on time dependent density functional theory. *J. Chem. Phys.* **2006**, *124*, 124520.
(78) Yomosa, S. Theory of the Excited State of Molecular Complex in Solution. *J. Phys. Soc. Jpn.* **1974**, *36*, 1655−1660.
(79) Bonaccorsi, R.; Cimiraglia, R.; Tomasi, J. Ab initio evaluation of absorption and emission transitions for molecular solutes, including separate consideration of orientational and inductive solvent effects. *J. Comput. Chem.* **1983**, *4*, 567−577.
(80) Cammi, R.; Corni, S.; Mennucci, B.; Tomasi, J. Electronic excitation energies of molecules in solution: State specific and linear response methods for nonequilibrium continuum solvation models. *J. Chem. Phys.* **2005**, *122*, 104513.
(81) Fukuda, R.; Ehara, M.; Nakatsuji, H.; Cammi, R. Non-equilibrium solvation for vertical photoemission and photoabsorption processes using the symmetry-adapted cluster−configuration interaction method in the polarizable continuum model. *J. Chem. Phys.* **2011**, *134*, 104109.
(82) Lunkenheimer, B.; Köhn, A. Solvent Effects on Electronically Excited States Using the Conductor-Like Screening Model and the Second-Order Correlated Method ADC(2). *J. Chem. Theory Comput.* **2013**, *9*, 977−994.
(83) Guido, C. A.; Jacquemin, D.; Adamo, C.; Mennucci, B. Electronic Excitations in Solution: The Interplay between State Specific Approaches and a Time-Dependent Density Functional Theory Description. *J. Chem. Theory Comput.* **2015**, *11*, 5782−5790.
(84) Alam, B.; Jiang, H.; Zimmerman, P. M.; Herbert, J. M. State-specific solvation for restricted active space spin−flip (RAS-SF) wave functions based on the polarizable continuum formalism. *J. Chem. Phys.* **2022**, *156*, 194110.
(85) David Sherrill, C.; Schaefer, H. F. In *Adv. Quantum Chem.*; Löwdin, P.-O., Sabin, J. R., Zerner, M. C., Brändas, E., Eds.; Academic Press, 1999; Vol. *34*; pp 143−269.
(86) Emrich, K. An extension of the coupled cluster formalism to excited states (I). *Nuclear Physics A* **1981**, *351*, 379−396.
(87) Sekino, H.; Bartlett, R. J. A linear response, coupled-cluster theory for excitation energy. *Int. J. Quantum Chem.* **1984**, *26*, 255−265.
(88) Cammi, R.; Mennucci, B. Linear response theory for the polarizable continuum model. *J. Chem. Phys.* **1999**, *110*, 9877.
(89) Corni, S.; Cammi, R.; Mennucci, B.; Tomasi, J. Electronic excitation energies of molecules in solution within continuum solvation models: Investigating the discrepancy between state-specific and linear-response methods. *J. Chem. Phys.* **2005**, *123*, 134512.

https://doi.org/10.1021/acs.jpca.4c03273
J. Phys. Chem. A 2024, 128, 6324−6335

(90) Guido, C. A.; Mennucci, B.; Scalmani, G.; Jacquemin, D. Excited State Dipole Moments in Solution: Comparison between State-Specific and Linear-Response TD-DFT Values. *J. Chem. Theory Comput.* **2018**, *14*, 1544−1553.
(91) Budzák, S.; Scalmani, G.; Jacquemin, D. Accurate Excited-State Geometries: A CASPT2 and Coupled-Cluster Reference Database for Small Molecules. *J. Chem. Theory Comput.* **2017**, *13*, 6237−6252.
(92) Marcus, R. A. Electrostatic Free Energy and Other Properties of States Having Nonequilibrium Polarization. I. *J. Chem. Phys.* **1956**, *24*, 979.
(93) Marcus, R. A. On the Theory of Oxidation-Reduction Reactions Involving Electron Transfer. I. *J. Chem. Phys.* **1956**, *24*, 966.
(94) Stein, T.; Kronik, L.; Baer, R. Reliable Prediction of Charge Transfer Excitations in Molecular Complexes Using Time-Dependent Density Functional Theory. *J. Am. Chem. Soc.* **2009**, *131*, 2818−2820.
(95) Baer, R.; Livshits, E.; Salzner, U. Tuned Range-Separated Hybrids in Density Functional Theory. *Annu. Rev. Phys. Chem.* **2010**, *61*, 85−109.
(96) Perdew, J. P.; Burke, K.; Ernzerhof, M. Generalized Gradient Approximation Made Simple. *Phys. Rev. Lett.* **1996**, *77*, 3865.
(97) Adamo, C.; Barone, V. Toward reliable density functional methods without adjustable parameters: The PBE0 model. *J. Chem. Phys.* **1999**, *110*, 6158.
(98) Goerigk, L.; Grimme, S. A thorough benchmark of density functional methods for general main group thermochemistry, kinetics, and noncovalent interactions. *Phys. Chem. Chem. Phys.* **2011**, *13*, 6670−6688.
(99) Refaely-Abramson, S.; Sharifzadeh, S.; Jain, M.; Baer, R.; Neaton, J. B.; Kronik, L. Gap Renormalization of Molecular Crystals from Density-Functional Theory. *Phys. Rev. B* **2013**, *88*, 081204.
(100) Joo, B.; Han, H.; Kim, E.-G. Solvation-Mediated Tuning of the Range-Separated Hybrid Functional: Self-Sufficiency through Screened Exchange. *J. Chem. Theory Comput.* **2018**, *14*, 2823−2828.
(101) Kimber, P.; Plasser, F. Toward an understanding of electronic excitation energies beyond the molecular orbital picture. *Phys. Chem. Chem. Phys.* **2020**, *22*, 6058−6080.
(102) Rohrdanz, M. A.; Herbert, J. M. Simultaneous benchmarking of ground- and excited-state properties with long-range-corrected density functional theory. *J. Chem. Phys.* **2008**, *129*, 034107.
(103) Rohrdanz, M. A.; Martins, K. M.; Herbert, J. M. A long-range-corrected density functional that performs well for both ground-state properties and time-dependent density functional theory excitation energies, including charge-transfer excited states. *J. Chem. Phys.* **2009**, *130*, 054112.
(104) Mardirossian, N.; Head-Gordon, M. ?B97M-V: A combinatorially optimized, range-separated hybrid, meta-GGA density functional with VV10 nonlocal correlation. *J. Chem. Phys.* **2016**, *144*, 214110.
(105) Caldeweyher, E.; Bannwarth, C.; Grimme, S. Extension of the D3 dispersion coefficient model. *J. Chem. Phys.* **2017**, *147*, 034112.
(106) Caldeweyher, E.; Ehlert, S.; Hansen, A.; Neugebauer, H.; Spicher, S.; Bannwarth, C.; Grimme, S. A generally applicable atomic-charge dependent London dispersion correction. *J. Chem. Phys.* **2019**, *150*, 154122.
(107) Friede, M.; Ehlert, S.; Grimme, S.; Mewes, J.-M. Do Optimally Tuned Range-Separated Hybrid Functionals Require a Reparametrization of the Dispersion Correction? It Depends. *J. Chem. Theory Comput.* **2023**, *19*, 8097−8107.
(108) Weigend, F.; Ahlrichs, R. Balanced basis sets of split valence, triple zeta valence and quadruple zeta valence quality for H to Rn: Design and assessment of accuracy. *Phys. Chem. Chem. Phys.* **2005**, *7*, 3297−3305.
(109) Weigend, F. Accurate Coulomb-fitting basis sets for H to Rn. *Phys. Chem. Chem. Phys.* **2006**, *8*, 1057−1065.
(110) Sun, H.; Zhong, C.; Brédas, J. L. Reliable Prediction with Tuned Range-Separated Functionals of the Singlet-Triplet Gap in Organic Emitters for Thermally Activated Delayed Fluorescence. *J. Chem. Theory Comput.* **2015**, *11*, 3851−3858.
(111) Jorner, K.; Pollice, R.; Lavigne, C.; Aspuru-Guzik, A. Ultrafast Computational Screening of Molecules with Inverted Singlet−Triplet Energy Gaps Using the Pariser−Parr−Pople Semiempirical Quantum Chemistry Method. *J. Phys. Chem. A* **2024**, *128*, 2445−2456.
(112) Ricci, G.; San-Fabián, E.; Olivier, Y.; Sancho-García, J. C. Singlet-Triplet Excited-State Inversion in Heptazine and Related Molecules: Assessment of TD-DFT and ab initio Methods. *ChemPhysChem* **2021**, *22*, 553−560.
(113) Becke, A. D. Singlet-triplet splittings from the virial theorem and single-particle excitation energies. *J. Chem. Phys.* **2018**, *148*, 044112.
(114) Kimber, P.; Plasser, F. Energy Component Analysis for Electronically Excited States of Molecules: Why the Lowest Excited State Is Not Always the HOMO/LUMO Transition. *J. Chem. Theory Comput.* **2023**, *19*, 2340.

https://doi.org/10.1021/acs.jpca.4c03273
J. Phys. Chem. A 2024, 128, 6324−6335